Cell

An Effector of RNA-Directed DNA Methylation in *Arabidopsis* Is an ARGONAUTE 4- and RNA-Binding Protein

Xin-Jian He,[1,6] Yi-Feng Hsu,[1,3,6] Shihua Zhu,[1,4] Andrzej T. Wierzbicki,[5] Olga Pontes,[5] Craig S. Pikaard,[5] Hai-Liang Liu,[1] Co-Shine Wang,[3] Hailing Jin,[2] and Jian-Kang Zhu[1,*]
[1]Institute for Integrative Genome Biology and Department of Botany and Plant Sciences
[2]Institute for Integrative Genome Biology and Department of Plant Pathology
University of California, Riverside, Riverside, CA 92521, USA
[3]Graduate Institute of Biotechnology, National Chung Hsing University, Taichung 40227, Taiwan
[4]College of Science and Technology, Ningbo University, Ningbo 315211, China
[5]Biology Department, Washington University, Campus Box 1137, One Brookings Drive, St. Louis, MO 63130, USA
[6]These authors contributed equally to this work
*Correspondence: jian-kang.zhu@ucr.edu
DOI 10.1016/j.cell.2009.04.028

SUMMARY

DNA methylation is a conserved epigenetic mark in plants and mammals. In *Arabidopsis*, DNA methylation can be triggered by small interfering RNAs (siRNAs) through an RNA-directed DNA methylation (RdDM) pathway. Here, we report the identification of an RdDM effector, KTF1. Loss-of-function mutations in *KTF1* reduce DNA methylation and release the silencing of RdDM target loci without abolishing the siRNA triggers. KTF1 has similarity to the transcription elongation factor SPT5 and contains a C-terminal extension rich in GW/WG repeats. KTF1 colocalizes with ARGONAUTE 4 (AGO4) in punctate nuclear foci and binds AGO4 and RNA transcripts. Our results suggest KTF1 as an adaptor protein that binds scaffold transcripts generated by Pol V and recruits AGO4 and AGO4-bound siRNAs to form an RdDM effector complex. The dual interaction of an effector protein with AGO and small RNA target transcripts may be a general feature of RNA-silencing effector complexes.

INTRODUCTION

RNA interference (RNAi) is a conserved gene-silencing mechanism in eukaryotic cells (Matzke and Birchler, 2005; Zaratiegui et al., 2007). In RNAi, double-stranded RNAs are processed by the RNaseIII enzyme Dicer into small interfering RNAs (siRNAs) that are then incorporated into an RNA-induced silencing complex (RISC) to direct the cleavage or translational inhibition of complementary RNA (Matzke and Birchler, 2005; Tomari and Zamore, 2005; Filipowicz, 2005). The core component of RISC is the PAZ- and PIWI-domain-containing protein, Argonaute (AGO), which binds to siRNAs and can slice complementary RNAs (Filipowicz, 2005; Qi et al., 2006). Similarly, miRNAs are also generated by Dicers and direct a miRNA RISC to cause degradation or translational inhibition of target mRNAs (Bartel, 2004). In fission yeast, siRNAs are incorporated into the RNA-induced transcriptional silencing (RITS) complex to cause heterochromatin formation (Volpe et al., 2002; Verdel et al., 2004). RITS also contains an AGO that slices transcripts complementary to the bound siRNAs (Verdel et al., 2004; Irvine et al., 2006). The conserved GW182 family of proteins is associated with miRNA RISC by binding to AGOs and is required for miRNA-mediated gene silencing (Ding and Han, 2007; Eulalio et al., 2008). In RITS, the Tas3 protein binds to AGO1 and is necessary for transcriptional gene silencing (Partridge et al., 2007; Till et al., 2007). The GW182 family of proteins and Tas3 all contain the GW/WG repeat sequence motif, which is considered an AGO hook that mediates interaction with AGOs (Ding and Han, 2007).

In plants, the overwhelming majority of small RNAs are 24 nt siRNAs corresponding to transposons and other repetitive elements (Zhang et al., 2007; Mosher et al., 2008). The 24 nt siRNAs cause epigenetic silencing by directing de novo DNA methylation through the RNA-directed DNA methylation (RdDM) pathway (Matzke and Birchler, 2005; Chan et al., 2005). In the RdDM pathway, siRNAs are generated by the action of the putative DNA-directed RNA polymerase Pol IV, RDR2 (RNA-dependent RNA polymerase 2), and DCL3 (Dicer-like 3) (Matzke et al., 2009). The siRNAs are loaded into AGO4 and AGO6 to direct DNA methylation by the de novo DNA methyltransferase DRM2 (Matzke et al., 2009). The functioning of the siRNAs also requires another putative DNA-dependent RNA polymerase, Pol V; the chromatin-remodeling protein, DRD1; and a structural-maintenance-of-chromosomes hinge domain-containing protein (Matzke et al., 2009). Pol IV and Pol V have distinct largest subunits, NRPD1 and NRPE1, respectively, but share with Pol II and/or with each other numerous additional subunits (Ream et al., 2009; Huang et al., 2009; He et al., 2009). NRPE1 contains a long C-terminal domain that is very rich in GW/WG repeats (El-Shami et al., 2007). The GW/WG repeats are required for

Pol V function and are both sufficient and necessary for interaction with AGO4 (El-Shami et al., 2007). Recently, Pol V was found to generate uncapped and nonpolyadenylated transcripts from several noncoding sequences that are targeted by RdDM (Wierzbicki et al., 2008). The evidence suggests that AGO4/6-bound siRNAs may find target DNA by binding to nascent scaffold transcripts generated by Pol V (Wierzbicki et al., 2009). The de novo DNA methyltransferase DRM2, which is presumably in the RdDM effector complex, is responsible for catalyzing cytosine methylation in CG, CHG, and CHH (H represents A, T, or C) sequence contexts (Cao and Jacobsen, 2002).

Active DNA demethylation mediated by the ROS1 family of DNA glycosylases is important for counteracting the activity of RdDM to prevent or attenuate hypermethylation and transcriptional silencing of transgene repeats, certain endogenous genes, transposons, and other repetitive sequences (Gong et al., 2002; Zhu et al., 2007; Penterman et al., 2007; Lister et al., 2008; He et al., 2009). In the DNA demethylase mutant *ros1*, these sequences show enhanced transcriptional silencing (Gong et al., 2002; Zhu et al., 2007; Lister et al., 2008). To identify RdDM pathway components, we carried out a genetic screen for second-site suppressors of the *ros1* mutant. Here, we report two allelic *ros1* suppressor mutants, *rdm3-1* and *rdm3-2*. The *rdm3* mutations release the silencing of an *RD29A* promoter-driven *luciferase* (*LUC*) transgene and the endogenous *RD29A* gene in *ros1* mutant plants. In the *rdm3* mutants, DNA methylation is reduced at RdDM target loci such as *5S rDNA*, *MEA-ISR*, *AtSN1*, *AtGP1*, and *AtMU1*. The *rdm3* mutations do not affect the levels of siRNAs corresponding to these loci, suggesting that RDM3 may function with Pol V in the effector step of RNA-directed DNA methylation. Like *ago4* mutations, however, *rdm3* does not block production of Pol V transcripts. *RDM3* encodes a protein that was annotated as KTF1 (KOW domain-containing transcription factor 1). KTF1 has similarity to SPT5, a conserved transcription elongation factor for RNA polymerase II (Wada et al., 1998; Winston, 2001). We found that KTF1 and AGO4 interact in vitro and in vivo, and the two proteins are colocalized in discrete nucleoplasmic foci. These results suggest that KTF1 may physically link Pol V transcription with AGO4-mediated transcript cleavage and epigenetic regulation. KTF1 contains a C-terminal region rich in WG repeats, and these repeats are sufficient for interaction with AGO4. Importantly, an RNA-binding site was identified in the C-terminal region of KTF1. We hypothesize that WG repeats have coevolved with an RNA-binding site in AGO-interacting proteins to facilitate the formation of a tight protein-transcript-siRNA effector complex for gene silencing.

RESULTS

The *rdm3* Mutations Suppress Transcriptional Gene Silencing in the *ros1* Mutant

Loss-of-function mutations in the DNA demethylase ROS1 cause transcriptional gene silencing (TGS) of the stress-responsive *RD29A* promoter-driven *luciferase* (*RD29A-LUC*) transgene, the endogenous *RD29A* gene, and the *CaMV 35S* promoter-driven *NPTII* (*35S-NPTII*) kanamycin resistance transgene that is physically linked to the *RD29A-LUC* transgene (Gong et al., 2002). The silencing of the *35S-NPTII* and *RD29A-LUC* transgenes is indicated by plant sensitivity to kanamycin and loss of luminescence, respectively. To identify components mediating TGS in *ros1*, we screened a T-DNA-mutagenized population in the *ros1* background, based on reactivation of luminescence from *RD29A-LUC* (He et al., 2009). Two allelic mutants, *rdm3-1* and *rdm3-2* (for RNA-directed DNA methylation 3), were characterized in this study.

Figure 1A shows the luminescence phenotypes of the wild-type, *ros1*, *ros1rdm3-1*, and *ros1rdm3-2*. Like the wild-type, both *ros1rdm3-1* and *ros1rdm3-2* emitted strong luminescence after cold treatment, whereas *ros1* emitted little or no luminescence. The result shows that the silencing of *RD29A-LUC* in *ros1* was suppressed by the *rdm3* mutations. However, the kanamycin sensitivity of *ros1rdm3-1* and *ros1rdm3-2* was similar to that of *ros1*, which indicated that the silencing of *35S-NPTII* in *ros1* was not suppressed by the *rdm3* mutations. The *ros1rdm3-1* and *ros1rdm3-2* double mutants were crossed to *ros1* (Figure 1A). The F1 plants emitted as little luminescence as the *ros1* plants, but the F2 progenies segregated ~3:1 for *ros1*:*ros1rdm3* luminescence phenotypes, suggesting that the *rdm3-1* and *rdm3-2* mutations were recessive and that each mutation was in a single nuclear gene (data not shown).

We crossed *ros1rdm3-1* plants to the wild-type and identified the *rdm3-1* single mutants. Interestingly, *rdm3-1* plants emitted stronger luminescence than the wild-type (Figures S1A and S1B available online). The result is consistent with the presence of a low level of TGS of the *RD29A-LUC* transgene in the wild-type (Gong et al., 2002; Agius et al., 2006) and suggests that RDM3 is required for this TGS.

As reported previously (Gong et al., 2002), the mRNA levels of the endogenous *RD29A*, *RD29A-LUC*, and *NPTII* transgenes were dramatically reduced by the *ros1* mutation. In *ros1rdm3-1*, the mRNA levels of both the endogenous *RD29A* and the *RD29A-LUC* transgene were substantially higher than those in *ros1* (Figure 1B). In contrast, the mRNA level of the *NPTII* transgene in *ros1rdm3-1* mutant was undetectable, as it was in *ros1*, which is consistent with the kanamycin-sensitive phenotype of the *ros1rdm3-1* and *ros1* plants (Figure 1B). These results demonstrate that the *rdm3* mutations suppress the TGS of the endogenous *RD29A* gene and the *RD29A-LUC* transgene, but not the *NPTII* transgene in the *ros1* mutant.

The *rdm3* Mutation Reduces DNA Methylation at the *RD29A* Promoter and Other RdDM Targets

To test whether the suppression of *RD29A-LUC* transgene silencing in the *ros1rdm3-1* mutant correlates with loss of DNA hypermethylation, we analyzed the DNA methylation status of the *RD29A* promoter by bisulfite sequencing. The results show that both the endogenous and transgenic *RD29A* promoters were heavily methylated at cytosine residues in all sequence contexts (CG, CHG, and CHH; H represents A, T, or C) in the *ros1* mutant, but the methylation was reduced in the *ros1rdm3-1* mutant (Figures 2A and 2B). The reductions were comparable to those in *ros1nrpd1* and were particularly evident at CHG and CHH sites (Figures 2A and 2B). For example, at the transgenic *RD29A* promoter, the asymmetric CHH methylation was 8.9% in the wild-type, 15.2% in *ros1*, 4.5% in *ros1rdm3-1*, and 2.8% in *ros1nrpd1* (Figure 2A). The methylation change at the

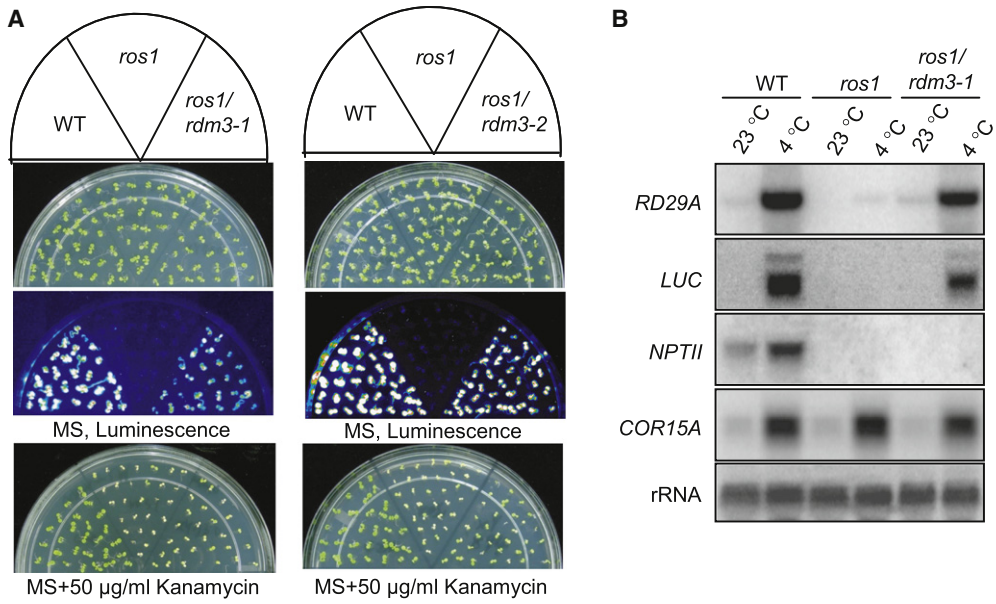

Figure 1. Transcriptional Gene Silencing of *RD29A-LUC* Is Suppressed by the *rdm3-1* and *rdm3-2* Mutations

(A) Effect of *rdm3-1* and *rdm3-2* on luminescence and kanamycin-resistance phenotypes in the *ros1* background. Plants were grown on MS plates and subjected to luminescence imaging after cold treatment (4°C, 24 hr). The plants were also grown on MS plates with kanamycin (50 μg/ml) and photographed after 10 days. (B) Northern blot analysis of RNA levels of endogenous *RD29A*, *RD29A-LUC*, and *35S-NPTII* in wild-type, *ros1*, and *ros1rdm3-1*. The constitutively expressed 18S rRNA was used as an RNA loading control, and *COR15A* was used as a cold treatment control.

endogenous *RD29A* promoter was also demonstrated by Southern hybridization (Figure S2A). Hypermethylation at the BstUI site of *RD29A* promoter in *ros1* prevented the methylation-sensitive restriction enzyme from cleaving the promoter. The partial cleavage in *ros1rdm3-1* and *ros1nrpd1* by BstUI thus indicates a reduction in DNA methylation (Figure S2A). The results suggest that, like *nrpd1*, *rdm3-1* suppresses the TGS in *ros1* by preventing DNA hypermethylation at the *RD29A* promoter.

The DNA methylation status of the highly repetitive 180 bp centromeric repeat, which is not controlled by RdDM, was analyzed by Southern hybridization. No difference in DNA methylation of the centromeric repeat was detected among wild-type, *rdm3-3* (a T-DNA allele from Stock Center, in the Col-0 background; Figure S3A), and *nrpe1-11* (*nrpd1b-11*) (Figure S2B). However, DNA methylation of 5S rDNA, an RdDM target locus, was reduced by the *rdm3* mutations at all cytosine contexts, similar to the effects of *nrpd1* and *nrpe1* (Figures S2C and S2D).

We then examined the methylation status of several other well-characterized RdDM target loci, including *AtSN1*, *MEA-ISR*, *AtMU1* and *AtGP1*. Bisulfite sequencing was used to examine DNA methylation at *AtSN1*, a retroelement, and at *MEA-ISR*, a subtelomeric repeat sequence present downstream of the *MEA* gene. The results show that, in the wild-type plants, *AtSN1* was heavily methylated with 66.1% of cytosine methylation at CG sites, 52.0% at CHG, and 5.2% at CHH but that the methylation levels were reduced to 50.0%, 14.3%, and 1.2%, respectively, in the *rdm3-3* mutant. This effect of the *rdm3-3* mutation on *AtSN1* methylation was similar to that of *nrpe1* (Figure 2C). Our bisulfite sequencing results also revealed that the DNA methylation level at *MEA-ISR* was reduced in *rdm3-3*, as it was in *nrpe1*, compared to that in the wild-type (Figure 2D).

The reduced methylation in *rdm3* mutants at CHH sites of *AtSN1* was further tested by digestion with the methylation-sensitive enzyme HaeIII, followed by PCR. Figure 2E shows that *AtSN1* was heavily methylated in wild-type and *ros1* and was thus resistant to HaeIII cleavage, but the methylation was much reduced in *ros1rdm3-1*, *ros1nrpd1*, and *ros1nrpe1* (Figure 2E). For analysis of the DNA methylation of *AtGP1* and *AtMU1*, the methylated DNA-digesting enzyme McrBC was applied, followed by PCR (Lippman et al., 2003). The results show that, like the *nrpd1* and *nrpe1* mutations, *rdm3-1* reduced the DNA methylation of *AtGP1* and *AtMU1* (Figure 2E). The effect of *rdm3* on DNA methylation at *AtSN1*, *AtGP1*, and *AtMU1* was confirmed by examining the *rdm3-3* allele (Figure S4A). Moreover, the methylation status of *AtMU1* at CHH sites was further tested by Southern hybridization, which showed that three HaeIII undigested bands in the wild-type were mostly digested in *rdm3-3*, *nrpd1*, and *nrpe1*, confirming the reduced *AtMU1* methylation in *rdm3* (Figure 2F). Taken together, our results show that *rdm3* mutations reduce DNA methylation at RdDM target sites and that the effect was similar to that of mutations in known RdDM components, such as *nrpd1*, *nrpe1*, *rdr2*, *dcl3*, and *ago4*.

The Effect of *rdm3* Mutations on 24 nt siRNAs and TGS of Transposons

The above results suggest that *RDM3* is required for DNA methylation at specific genomic loci. By semiquantitative RT-PCR, we tested whether the reduction of DNA methylation at *AtSN1*, *AtGP1*, and *AtMU1* in *rdm3* mutant plants resulted in elevated

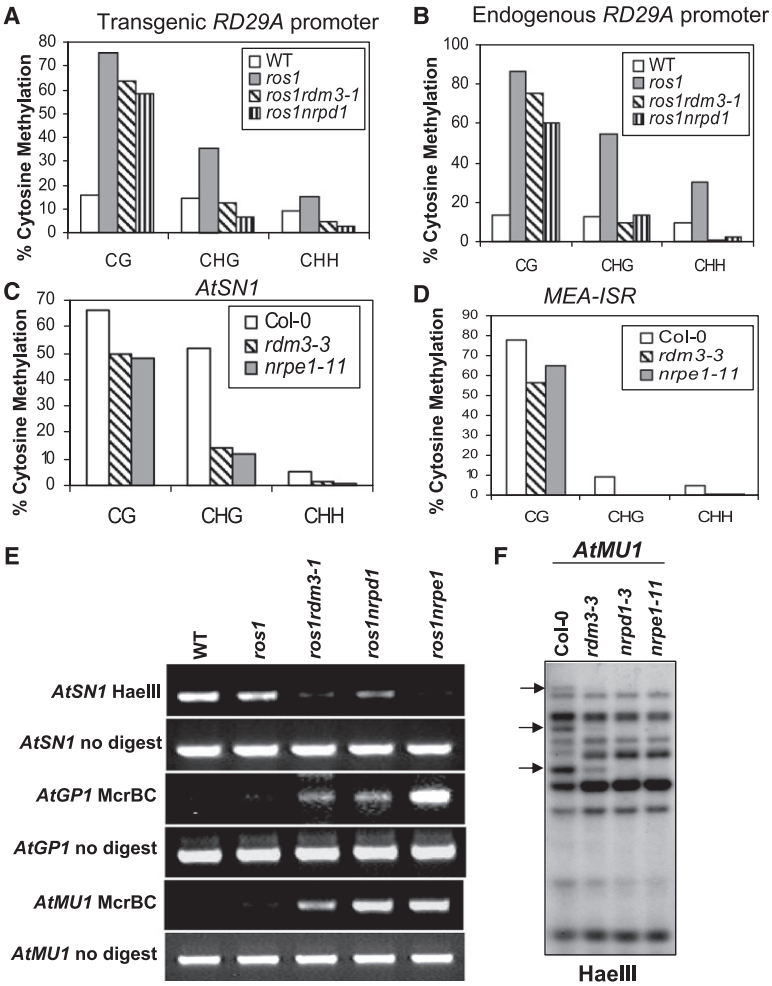

Figure 2. The *rdm3* Mutations Reduce DNA Methylation at RdDM Target Loci

(A–D) The percentage of cytosine methylation was determined by bisulfite sequencing at transgenic (A) and endogenous (B) *RD29A* promoters, *AtSN1* (C) and *MEA-ISR* (D). The percentage of cytosine methylation on CG, CHG, and CHH sites is shown. H represents A, T, or C.

(E) The *rdm3-1* mutation suppressed DNA methylation in *AtSN1*, *AtGP1*, and *AtMU1*. After the indicated genomic DNA was digested with the methylation-sensitive restriction enzyme HaeIII, it was used for amplification of *AtSN1*. After the genomic DNA was digested with the methylated DNA-specific restriction enzyme McrBC, it was used for amplification of *AtGP1* and *AtMU1*. The amplifications of nondigested genomic DNA were used as controls.

(F) The *rdm3-3* mutation reduced *AtMU1* methylation at CHH sites. Genomic DNA from the indicated genotypes was digested with HaeIII, followed by Southern blot analysis. The three undigested bands (arrows) that are present in the Col-0 wild-type were mostly digested in *rdm3-3*, *nrpd1-3*, and *nrpe1-11*.

transcript levels from these loci. The *AtSN1* transcript level was compared among the wild-type Col-0, *rdm3-3*, *nrpd1*, and *nrpe1* mutant plants. The results show that a very low level of *AtSN1* transcript was detected in the Col-0 wild-type but that the transcript level was drastically increased in *rdm3-3*, as well as in *nrpd1* and *nrpe1* (Figure 3A). Similarly, *AtGP1* and *AtMU1* had very low transcript levels in the wild-type and *ros1*, but the transcript levels were substantially increased in *ros1rdm3-1*, as well as in *ros1nrpd1* and *ros1nrpe1* (Figure 3A). The results suggest that loss of DNA methylation caused by the *rdm3* mutations leads to a release of TGS at the RdDM target loci.

Our previous studies suggested that 24 nt siRNAs from the *RD29A* promoter are the trigger for TGS of *RD29A-LUC* and endogenous *RD29A* in *ros1* (Gong et al., 2002; Zheng et al., 2007; He et al., 2009). To determine whether *rdm3* mutations affect siRNA accumulation, we carried out small RNA blot analysis and found that the *rdm3-1* mutation has no effect on the accumulation of 24 nt *RD29A* promoter siRNAs, whereas *nrpd1* blocks the siRNAs and *nrpe1* partially reduces them (Figure 3B). The results indicate a role for RDM3 that is downstream of siRNA production in the RdDM pathway. We also tested the effect of *rdm3* on endogenous siRNAs from several other RdDM target loci, including *AtSN1*, 5S rDNA, Cluster 4, *AtGP1*, and *AtMU1* (Figures 3B and S4B). The siRNA1003 from 5S rDNA was not affected in *ros1rdm3-1*, although it was blocked in *ros1nrpd1* and partially reduced in *ros1nrpe1*. The siRNAs from *AtGP1*, *AtMU1*, and Cluster 4 were mostly unaffected in *ros1rdm3-1* and *ros1nrpe1*, although they were eliminated in *ros1nrpd1* (Figure 3B). The *AtGP1*, *AtMU1*, 5S rDNA, and Cluster 4 siRNA results were further confirmed in *rdm3-3* (Figure S4B). In addition, *AtSN1* siRNAs and siRNA02 were not reduced by the *rdm3-3* mutation (Figure S4B). The 21 nt miRNA171 and ta-siRNA siRNA255 were also tested, and the results show that the *rdm3* mutations had no effect on either of them (Figures 3B and S4B). These results suggest that RDM3 acts in the RdDM pathway downstream of siRNA production, and thus, like NRPE1 (Pol V), RDM3 can be considered as an effector of RdDM.

The *rdm3-3* Mutation Does Not Block the Accumulation of Pol V-Dependent Noncoding Transcripts

To further delineate the role of RDM3 in the RdDM pathway, we tested whether RDM3 is required for the accumulation of Pol V-dependent transcripts (Wierzbicki et al., 2008). Pol V-dependent transcripts at *IGN5*, *IGN6*, and *AtSN1* loci (intervals B and C) were still detectable in the *rdm3-3* mutant (Figure 3C). In fact, the *IGN5* transcript level was slightly increased in *rdm3-3* (Figure 3C). Pol II and Pol III transcripts at the *solo LTR* and *AtSN1* (interval A) loci, respectively, were upregulated in *nrpe1* and were also upregulated in the *rdm3-3* mutant (Figure 3C).

The *RD29A* promoter generates 24 nt siRNAs and is targeted by the RdDM pathway for silencing (Gong et al., 2002; He et al., 2009). We found that the *RD29A* promoter also generated an RNA transcript that requires NRPE1 (Figure 3D). This Pol V-dependent *RD29A* promoter transcript was present in *ros1rdm3-1*, as well as in *ros1* and the wild-type (Figure 3D).

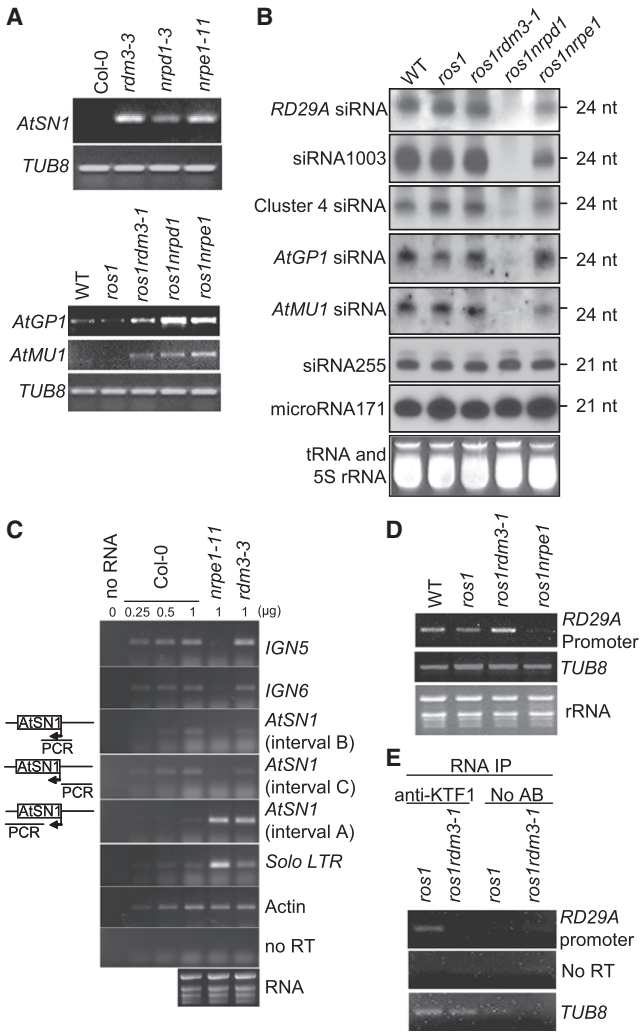

Figure 3. Effect of the *rdm3* Mutations on RNA and siRNA Levels from the RdDM Target Loci

(A) The *rdm3* mutations increase the RNA expression levels of *AtSN1*, *AtGP1*, and *AtMU1*. Semiquantitative RT-PCR was used to detect the transcript levels of *AtSN1* (interval A, see diagram in panel [C]), *AtGP1*, and *AtMU1* in the indicated genotypes. *TUB8* was amplified as an internal control.

(B) Small RNA blot analysis of 24 nt siRNAs, 21 nt ta-siRNAs, and microRNAs in the various genotypes. The positions of size markers (21 nt and 24 nt) are indicated. The ethidium bromide-stained small RNA gel is shown as a loading control.

(C) Strand-specific RT-PCR analysis of *IGN5*, *IGN6*, *AtSN1*, and *solo LTR* transcripts in the Col-0 wild-type, *nrpe1-11*, and *rdm3-3*. Actin PCR products and total RNA resolved by agarose gel electrophoresis serve as loading controls. Reactions without reverse transcriptase (no RT) were performed to control for background DNA contamination. The positions of the different *AtSN1* intervals tested by RT-PCR are indicated in the diagram on the left.

(D) RT-PCR analysis of *RD29A* promoter transcript. *TUB8* and ethidium bromide-stained gel are shown as controls.

(E) RT-PCR detection of *RD29A* promoter transcript in KTF1 immunoprecipitates. The background signal from *TUB8* was used as an internal control, which indicated no difference between the RNA amounts from *ros1* and *ros1rdm3-1*. No AB, controls without using anti-KTF1 antibody.

Collectively, these data suggest that RDM3 affects RdDM at a step downstream, or independent, of Pol V transcription.

RDM3 Encodes the KTF1 Protein, a SPT5-like Transcription Elongation Factor with a C-Terminal Extension Rich in WG/GW Repeats

To clone the *RDM3* gene, we used TAIL-PCR to determine the T-DNA insertion site in the *ros1rdm3-1* mutant and found a single T-DNA insertion in the first intron of AT5G04290 (Figure S3A). In the *ros1rdm3-2* mutant, we found a 61 bp deletion in the seventh exon of AT5G04290 (Figure S3A). We obtained the *rdm3-3* mutant from the SALK collection (Salk_001254), which has a T-DNA insertion in the tenth exon of AT5G04290 (Figure S3A). In *rdm3-3*, DNA methylation was dramatically reduced at several tested genomic loci, including *AtSN1*, *AtGP1*, *AtMU1*, *5S rDNA*, and *MEA-ISR* (Figures 2C, 2D, 2F, S2C, S2D, S3C, and S4A). These multiple mutations indicate that AT5G04290 is the *RDM3* gene. AT5G04290 was annotated as KTF1 (KOW domain-containing transcription factor 1) (http://www.arabidopsis.org/servlets/TairObject?id=136799&type=gene). The identity of the *RDM3* gene was confirmed by complementation tests in which introduction of a *KTF1* genomic fragment from the wild-type restored the silencing of *RD29A-LUC* and *AtSN1* methylation in *ros1rdm3-1* and *rdm3-3* (Figures S3B and S3C).

A cDNA containing the entire open reading frame of *KTF1* was cloned. Based on the sequence of the cloned cDNA, the *KTF1* gene contains 18 exons (Figure S3A) and encodes a protein of 1476 amino acid residues (Figure 4A). This differs from the computational gene structure prediction on the TAIR website (http://www.arabidopsis.org/servlets/TairObject?id=136799&type=gene). RT-PCR assays showed that the three *rdm3* mutations blocked the accumulation of full-length *KTF1* transcripts (Figure S5A). Western blot analysis revealed a lack of the KTF1 protein in *ros1rdm3-1* and *rdm3-3* mutant plants (Figure S5B). These results suggest that the three *rdm3* mutants are null alleles.

The KTF1 protein is highly similar to the SPT5 family of transcription elongation factors in its N-terminal region (Figure S6A). SPT5 is an essential gene conserved in all eukaryotes and is known to play both positive and negative roles in transcription elongation (Winston, 2001; Yamada et al., 2006). SPT5 proteins contain an acidic domain at the N-terminal region in addition to NusG and KOW domains and C-terminal repeats (Ivanov et al., 2000). KTF1 lacks an acidic N terminus, and its C-terminal region is different from that of SPT5 proteins, so its similarity to SPT5 proteins is restricted to the NusG and KOW domains. Phylogenetic analysis shows that KTF1 and its orthologs from other plants, including rice and grape, are more closely related to SPT5 orthologs from plants and animals than to SPT5 proteins from yeasts (Figure S6B). Consistent with a role of KTF1 in RdDM, KTF1 contains a putative nuclear localization signal (NLS) near the N terminus (Figure 4A). The long C-terminal region of KTF1 is characterized by more than 40 WG-containing repeats (Figure 4A). A large number of WG/GW repeats are also present in the C-terminal region of the largest subunit of Pol V, NRPE1, and in GW182 and related proteins in metazoans (El-Shami et al., 2007; Ding and Han, 2007; Eulalio et al., 2008). The fission yeast Tas3 protein also contains several WG/GW repeats (Till et al., 2007; Partridge et al., 2007). WG/GW-containing sequences

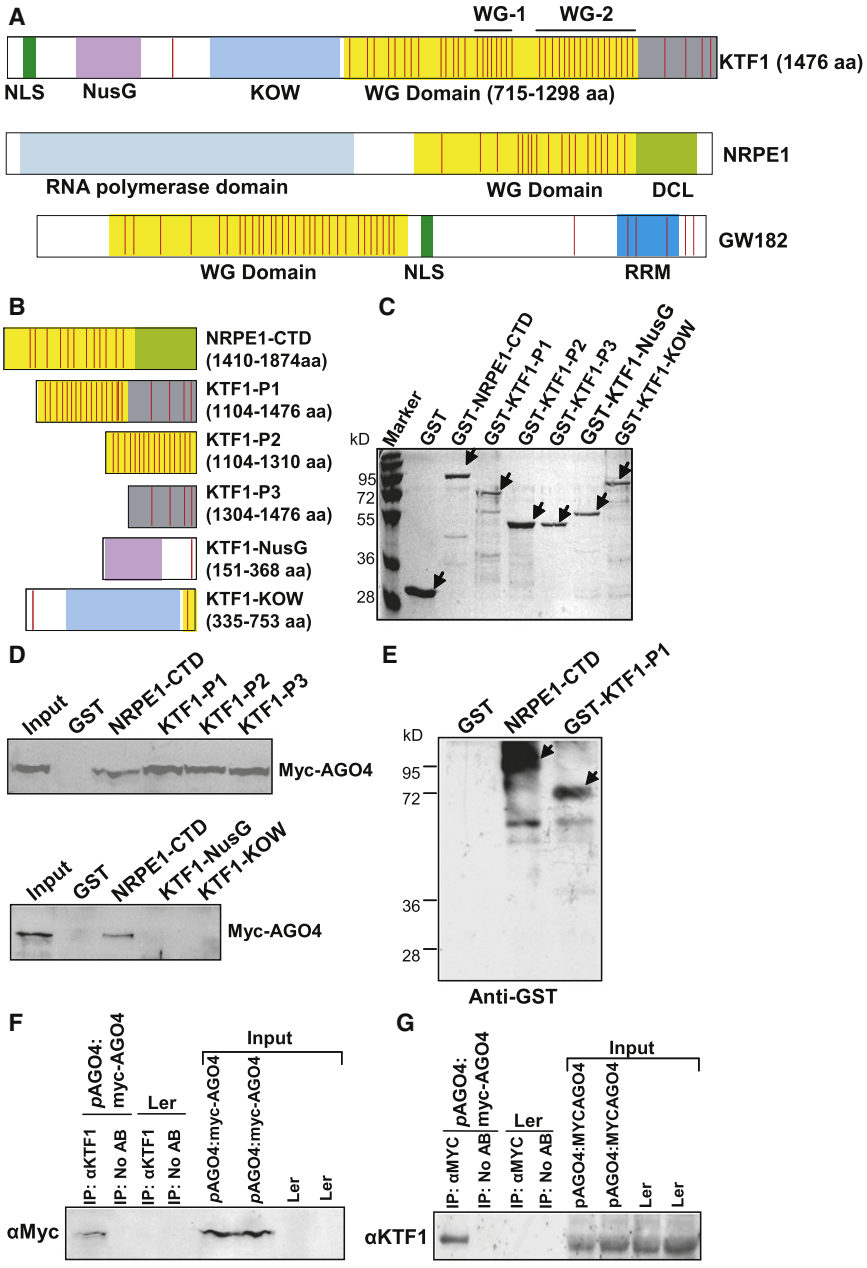

Figure 4. The WG/GW Repeats in KTF1 C-Terminal Domain Interact with AGO4

(A) KTF1, NRPE1, and HsGW182 proteins are shown schematically. All three proteins are characterized by the reiterated WG/GW repeat-containing domains (in yellow). The red stripes represent each of the WG/GW repeats. WG-1 and WG-2 represent two highly conserved WG repeat regions in KTF1.

(B) Diagram of the bacterially expressed NRPE1-CTD and truncated KTF1 proteins.

(C) The purified proteins were subjected to SDS-PAGE, and gels were stained with Coomassie. Arrows point to the proteins of interest.

(D) Western blot analysis showing that the GST-fused truncated KTF1 and NRPE1-CTD interact with Myc-AGO4 from plant extracts. Ten percent of the input was used in the "Input" lane.

(E) Anti-Myc antibody-conjugated beads captured truncated KTF1 proteins and NRPE1-CTD from a mixture of the proteins with extract from *Myc-AGO4* plants. Arrows point to the proteins of interest.

(F and G) Western blot analysis showing coimmunoprecipitation of KTF1 and Myc-AGO4. Ler wild-type plants without the *Myc-AGO4* transgene were used as controls. No AB, control precipitation without using antibodies.

are not conserved beyond the defining WG/GW core pattern, even between orthologous proteins. However, part of the WG repeat region of KTF1 is similar to the WG repeat region in Tas3, including residues surrounding the WG sequences (Figure S6C). There are 42 WG repeats in KTF1, and most of them are clustered in the C-terminal region of the protein as diagrammed in Figure 4A. As in NRPE1 (El-Shami et al., 2007), the WG repeat domain in KTF1 is highly hydrophilic and rich in G, S, D, K, and W (Table S1). The WG repeats are concentrated in two subdomains in the C-terminal region of KTF1, which are designated WG-1 and WG-2 (Figure 4A); WG-1 has seven highly conserved WG repeats, and WG-2 has 15 such repeats (Figure S6D).

KTF1 Interacts with AGO4 via Its WG Repeat Domain

Recently, it was discovered that WG/GW repeats in *Arabidopsis* NRPE1, animal GW182 (Figure 4A) and its paralogs, and the fission yeast Tas3 serve as AGO-binding motifs (El-Shami et al., 2007; Eulalio et al., 2008; Ding and Han, 2007; Till et al., 2007; Partridge et al., 2007). To determine whether the C-terminal WG repeat region of KTF1 can provide binding sites for AGO4, we generated GST-KTF1 fusion constructs (GST-KTF1-P1, -P2, and -P3) and produced truncated versions of KTF1 (Figure 4B). The C-terminal region of NRPE1 was used as a positive control (NRPE1-CTD; Figure 4B). The bacterially produced GST fusion proteins were purified (Figure 4C) and used to capture Myc-AGO4 from the crude protein extracts from *Myc-AGO4* transgenic plants. Myc-AGO4 was captured by all three versions of truncated KTF1 proteins from the C-terminal region, as well as by NRPE1-CTD, but was not captured by the two truncated KTF1 proteins (KTF1-NusG and KTF1-KOW) from the conserved NusG and KOW domains (Figure 4D). As expected, Myc-AGO4 was not captured by the negative control protein, GST (Figure 4D). Because RNase was present in the binding assay, the capture of Myc-AGO4 by the GST fusion proteins (GST-KTF1-P1, -P2, and -P3) was probably due to direct interactions between AGO4 and the truncated KTF1 proteins rather than indirect interactions mediated by scaffold RNA transcripts. We also

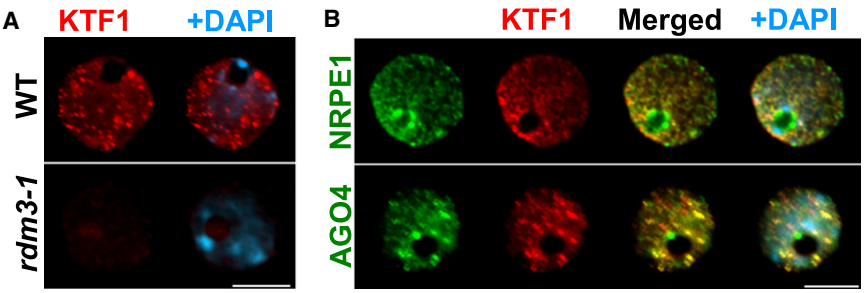

Figure 5. Subnuclear Localization of KTF1 in Interphase *Arabidopsis* Nuclei

(A) Detection of KTF1 (in red) in wild-type (WT) and *rdm3-1* mutant nuclei by immunofluorescence using anti-KTF1.

(B) Simultaneous localization of KTF1 and AGO4 or NRPE1. KTF1 (red) was localized using its specific antibody in cells expressing cMyc- and Flag-tagged AGO4 and NRPE1 (in green), respectively. The bright yellow signals due to the overlap of red and green channels in merged images indicate colocalization of two labeled proteins.

In all panels, DNA was stained with DAPI (blue). Scale bars, 5 μm.

used anti-Myc antibodies to capture bacterially purified GST-KTF1-P1 and GST-NRPE1-CTD after mixing the recombinant proteins with crude protein extracts from *Myc-AGO4*-transgenic plants. The result shows that GST-KTF1-P1 and GST-NRPE1-CTD, but not GST, were captured by the Myc antibodies (Figure 4E). These results demonstrate that KTF1 and AGO4 interact in vitro and that only a few WG repeats from KTF1 are sufficient for the interaction because KTF1-P3 contains only four WG/GW repeats. In the fission yeast Tas3 protein, one or two WG repeats are sufficient for binding to Ago1 (Partridge et al., 2007; Till et al., 2007). Nevertheless, KTF1-NusG and KTF1-KOW did not interact with AGO4, although the truncated proteins have one and two WG motifs, respectively (Figures 4B and 4D). Perhaps the hydrophilic amino acid residues in the WG repeat domain of KTF1 are also required for AGO4 interaction.

We performed coimmunoprecipitation experiments to test whether KTF1 interacts with AGO4 in vivo. Myc-AGO4 was detected in KTF1 immunoprecipitates from *Myc-AGO4*-transgenic plants (Figure 4F). Likewise, KTF1 was detected in Myc-AGO4 immunoprecipitates (Figure 4G). The result suggests that KTF1 and AGO4 interact in vivo.

Partial Colocalization of KTF1 with AGO4 and Pol V in the Nucleoplasm

To visualize the subnuclear localization of KTF1, we performed immunostaining in interphase nuclei using antibodies specific for KTF1. In 100% of labeled nuclei (n = 123), KTF1 immunosignals show distinct nucleoplasmic foci but no nucleolar localization in wild-type leaves (Figure 5A). In the *rdm3-1* mutant, the signal intensity is strongly reduced (Figure 5A, 100% of the nuclei, n = 97), confirming that the KTF1 antibody is specific.

In order to determine whether KTF1 might be associated with AGO4 and Pol V in vivo in the nucleus, we performed coimmunolocalization experiments using antibody against the native KTF1 protein and transgenic lines expressing NRPE1-Flag and Myc-AGO4. Both NRPE1 and AGO4 are localized to the nucleoplasm but also display an intense, round-shaped nucleolar signal (Figure 5B) as described previously (Pontes et al., 2006; Li et al., 2006). The merging of KTF1 and AGO4 signals showed a similar distribution pattern and colocalization in the same nucleoplasmic sites, but not in the nucleolus, as indicated by the yellow signals (Figure 5B) in most of the cells (81%, n = 147). With respect to KTF1 and NRPE1, the majority of cells (63%, n = 135) also showed a partial colocalization of the two proteins in the nucleoplasm, but not in the nucleolus or nucleolar periphery (Figure 5B). These colocalization results are consistent with a physical interaction between KTF1 and AGO4 in vivo in the nucleoplasm. There may also be an interaction between KTF1 and NRPE1, albeit to a lesser extent.

KTF1 Is an RNA-Binding Protein

In electrophoretic mobility shift assays (EMSA), the C-terminal region of KTF1 (i.e., KTF1-P1) displays an RNA-binding activity. KTF1-P1, but not GST, could bind to 40 nt single-stranded RNA corresponding to the *RD29A* promoter (part of the Pol V-dependent *RD29A* promoter transcript) (Figure S7A). Interestingly, KTF1-P3, but not KTF1-P2, was also capable of binding to the RNA (Figure 6A). Because KTF1-P2 contains many more WG repeats than does KTF1-P3, the results indicate that WG repeats are not responsible for RNA binding. KTF1-P1 and KTF1-P3, but not GST or KTF1-P2, also bound to a 24 nt RNA, which corresponds to part of the 40 nt RNA (Figure S7B). Similarly, KTF1-P3, but not GST or KTF1-P2, was capable of binding to a 21 nt RNA (Figure S7C). Very strong binding was observed for KTF1-P3 to 500 nt RNA corresponding to the *RD29A* promoter (Figure 6B). KTF1-P3 was capable of binding to not only the 40 nt RNA, but also to its complementary RNA (Figure 6C). These results show that KTF1 can bind RNAs of various sizes and that the binding is not sequence or strand specific.

KTF1-P3 bound to the 40 nt Pol V transcript in a dose-dependent manner (Figure 6D). The binding was reduced or blocked by competition with unlabeled RNA of the same sequence (Figure 6D). KTF1-P3 did not bind to 40 nt DNA of the same sequence as the RNA (Figure 6E). Furthermore, KTF1-P3 specifically bound to the 40 nt single-stranded RNA and did not bind to the corresponding double-stranded RNA (Figure 6F).

To test whether KTF1 may be associated with Pol V transcripts in vivo, RNA immunoprecipitation was carried out using anti-KTF1 antibodies. The Pol V-dependent transcript from the *RD29A* promoter was detected in the KTF1 immunoprecipitate from *ros1*, but not from *ros1rdm3-1* (Figure 3E). No signal was detected in *ros1* or *ros1rdm3-1* following precipitation in the absence of the anti-KTF1 antibody. Taken together, the results suggest that KTF1 can bind to the Pol V-dependent *RD29A* promoter transcript in vitro and in vivo.

DISCUSSION

Our genetic analysis indicates that KTF1 is a critical effector in the RdDM pathway. Like most of the previously identified

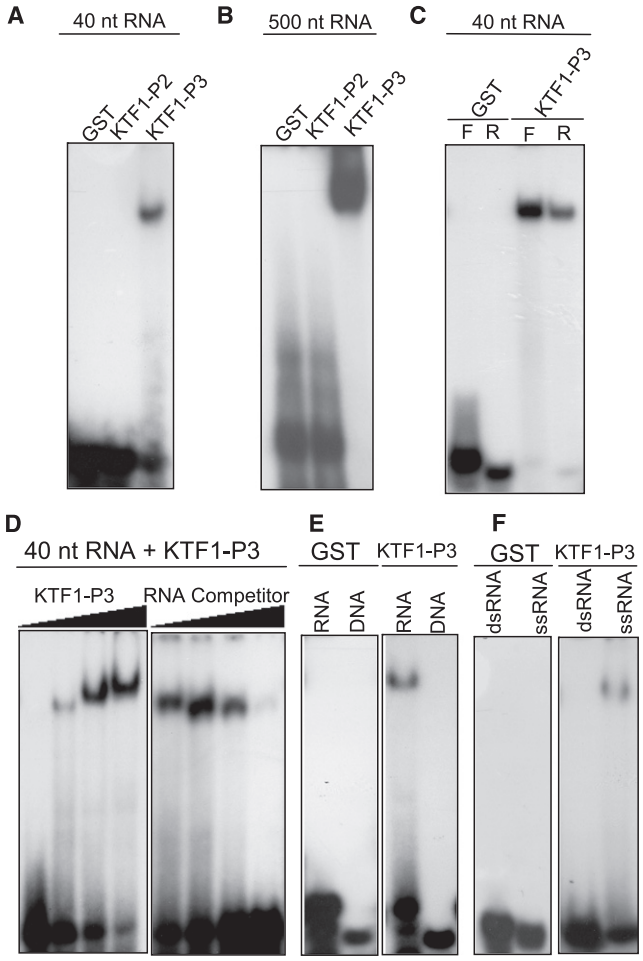

Figure 6. The KTF1 C-Terminal Domain Binds RNAs

(A) KTF1-P3, but not KTF1-P2, binds to a 40 nt RNA (corresponding to the *RD29A* promoter) in electrophoretic mobility shift assays.

(B) KTF1-P3, but not KTF1-P2, binds to a 500 nt RNA corresponding to the *RD29A* promoter.

(C) KTF1-P3 binds to both the forward (F) and reverse (R) strands of the 40 nt RNA.

(D) Protein concentration dependence of the RNA binding and competition by unlabeled RNA. The protein-RNA complex increased when an increasing amount of KTF1-P3 protein (0.2, 0.4, 0.8, and 1.6 μg) was added to the binding reaction. The protein-RNA complex decreased when an increasing amount of unlabeled 40 nt RNA (1×, 5×, 25×, and 125× of labeled RNA) was added to the binding reaction.

(E) KTF1-P3 binds to the 40 nt RNA but does not bind to DNA of the same sequence.

(F) KTF1-P3 binds to the single-stranded, but not double-stranded, 40 nt RNA.

RdDM components (He et al., 2009), KTF1 is required for TGS of the *RD29A-LUC*, but not of the *35S-NPTII* transgene, suggesting that KTF1 functions specifically in siRNA-dependent, but not siRNA-independent, TGS. KTF1 contains the NusG and KOW domains that are highly conserved in the SPT5 family of proteins from yeast to humans. In humans, SPT5 is involved in transcriptional inhibition mediated by 5, 6-dichloro-1-beta-D-ribofuranosylbenzimidazole (DRB) (Wada et al., 1998). SPT5 and SPT4 form a heterodimeric complex that is also known as DSIF (DRB sensitivity-inducing factor) (Wada et al., 1998). DSIF can regulate transcription elongation in both positive and negative manners by regulating the processivity of RNA polymerase II (Wada et al., 1998; Yamada et al., 2006).

Considering its specific role in the RdDM pathway, KTF1 may regulate Pol V transcription. Recently, Huang et al. (2009) reported that KTF1 could be detected in Pol V complexes purified from the inflorescence tissue of cauliflower, and T-DNA insertion mutants in this gene in *Arabidopsis* had reduced DNA methylation at several RdDM target loci. We found that Pol V transcripts are not blocked by the *rdm3* mutation (Figures 3C and 3D). Therefore, unlike Pol V, KTF1 is not required for generating the noncoding transcripts. In Pol II transcription, SPT5 interacts with Pol II and RNA-processing factors and is also associated with the exosome (Lindstrom et al., 2003). Thus, SPT5 is involved in the coordination between transcription elongation and RNA processing and degradation. Our results show that KTF1 interacts with AGO4, another effector of RdDM. AGO4 binds siRNAs, and its slicer activity cleaves at least some target RNA transcripts (Qi et al., 2006). This cleavage activity is required for de novo methylation at some RdDM target loci (Qi et al., 2006). Therefore, our results suggest that KTF1 is involved in coordinating Pol V transcription elongation with AGO4-mediated transcript binding or cleavage.

Our data show that KTF1 is an RNA-binding protein. KTF1 is capable of binding Pol V transcripts in vitro and in vivo (Figures 6 and 3E). KTF1 binding to Pol V transcripts is presumably important for the assembly of a functional RISC-like complex containing AGO4, AGO4-bound siRNAs, and Pol V transcripts complementary to the siRNAs. The interaction between an AGO-bound small RNA and its target transcript alone may not be sufficient for the assembly of a functional effector complex, and an adaptor protein like KTF1 that binds to both the AGO and target transcript may be needed. In metazoans, the P body constituents GW182 and the related TNRC6B and TNRC6C proteins are important for miRNA RISC function (Ding and Han, 2007). These proteins contain not only GW/WG repeats for interacting with AGOs, but also RNA recognition motifs (RRM) for binding miRNA-targeted mRNAs. This dual interaction of GW182 with AGO and target transcripts of small RNAs may be important for efficient location of target transcripts by AGO-bound small RNAs and for the assembly of a functional RISC to silence the target transcripts. In the RITS complex in fission yeast, Tas3 contains WG repeats and interacts with Ago1 (Verdel et al., 2004; Partridge et al., 2007; Till et al., 2007). The targeting of the Clr4 methyltransferase complex (ClrC) is closely coupled to transcription of the target loci, and Tas3 is required for the physical interaction between ClrC and RITS (Chen et al., 2008; Zhang et al., 2008). Although Tas3 has not yet been reported to bind RNA transcripts, artificial tethering of Tas3, but not any other components of RITS, to a nascent reporter transcript caused the silencing of the tethered transcript (Buhler et al., 2006). It is possible that Tas3 may contain an as yet unidentified RNA-binding site. We propose that the effector complex of various small RNA-mediated silencing pathways may contain an adaptor protein capable of bridging AGO and target transcripts of the small RNAs. In this regard, an RNA-binding site may have coevolved with the AGO-binding WG/GW repeats in

KTF1, GW182, and other related adaptor proteins in silencing effector complexes.

In the RdDM pathway, the NRPE1 subunit of Pol V also contains many WG/GW repeats in the C-terminal domain that binds to AGO4 (El-Shami et al., 2007). Like KTF1, the C-terminal domain of NRPE1 can also bind RNA transcripts (X.-J.H., Y.-F.H., and J.-K.Z., unpublished data). The noncoding transcripts produced by Pol V and bound to NRPE1 may be cleaved by the NRPE1-associated AGO4. The cleaved transcripts may be transferred to KTF1, which attracts additional AGO4 with bound siRNAs. This transcript-KTF1-AGO4-siRNA complex may then recruit DRM2 to cause de novo methylation of the noncoding transcripts-generating loci. Future experiments will be able to test this speculative model.

EXPERIMENTAL PROCEDURES

Plant Growth, Mutant Screening, and Gene Cloning

The wild-type C24 and the *ros1* mutant plants carry a homozygous stress-responsive *RD29A-LUC* transgene (He et al., 2009). A T-DNA mutagenized population in the *ros1* background was generated as described previously (Kapoor et al., 2005). Screening for *ros1* suppressors and isolation of T-DNA-tagged gene by TAIL-PCR (*rdm3-1*) and of untagged gene (*rdm3-2*) by map-based cloning were as described previously (He et al., 2009). An ~8.8 kb *KTF1* genomic fragment was amplified from Col-0 wild-type plants and cloned into the Gateway vector PMDC164 for complementation assay in *ros1rdm3-1* and *rdm3-3*.

DNA Methylation Assay

The DNA methylation status was analyzed by Chop-PCR, Southern hybridization, and bisulfite sequencing. For Chop-PCR, genomic DNA (500 ng) was digested with the methylation-sensitive restriction enzyme HaeIII overnight or the methylated DNA-digesting enzyme McrBC for 1 hr. The digested DNA was used to amplify the RdDM targets, including *AtSN1*, *AtGP1*, and *AtMU1*. The undigested genomic DNA was simultaneously amplified as controls. Southern hybridization and bisulfite sequencing were carried out as described in He et al. (2009).

RNA Analysis

RNA blot assays were carried out as described in He et al. (2009). The sequences of DNA oligo probes and primers for probe amplification are listed in Table S2.

For semiquantitative RT-PCR analysis, we extracted total RNA from flowers using Trizol reagent (Invitrogen). After contaminating DNA was removed by DNase, 5 μg of total RNA was used for synthesis of cDNA with SuperScript III (Invitrogen). The cDNA reaction mixture was diluted and used for RT-PCR. The PCR conditions were: 95°C for 5 min followed by 28–35 amplification cycles (95°C for 30 s, 56°C for 30 s, and 72°C for 1 min). The constitutively expressed *TUB8* was used as an internal control. Primers used in RT-PCR are listed in Table S2. Conditions and primers for RT-PCR analysis of Pol V-dependent transcripts are as described in Wierzbicki et al. (2008).

Binding Assay of GST Fusion Proteins and Myc-AGO4

The NRPE1-CTD (1410–1874 aa) and the five truncated forms of KTF1 (1104–1476 aa; 1104–1310 aa; 1304–1476 aa; 151–368 aa; and 335–753 aa) were amplified and cloned into bacterial expression vector pGEX4T1 (Invitrogen). The constructs were transformed into *E. coli*-competent cells BL21 for expression. The GST fusion proteins were purified by glutathione Sepharose 4B beads (Amersham) and used for binding assays as described previously (Li et al., 2006). In brief, a total of 150 μl of protein extract from flowers was added to the GST fusion protein beads (in bacterial protein extraction buffer containing DNase and RNase) and incubated at 4°C for 3 hr. The bound proteins were eluted with SDS-PAGE sample buffer after the beads were washed with IP buffer three times. Anti-Myc-conjugated agarose (Upstate) was used for immunoprecipitating Myc-AGO4 complexes from cell lysates mixed with purified GST fusion proteins at 4°C for 3 hr. The immunoprecipitated protein was eluted with SDS-PAGE sample buffer. All of the eluted protein was subjected to 10% SDS-PAGE gel for western blotting.

Coimmunoprecipitation of AGO4 and RDM3

One gram of flowers from *Myc-AGO4* transgenic plants (Li et al., 2006), as well as from the wild-type plants, was used for preparation of cell lysates with 2 ml of protein extraction buffer. Equal amounts of crude protein extracts were precleared with protein A agarose beads (Sigma), followed by anti-KTF1 or anti-Myc incubation. The immunoprecipitated protein complexes were captured with protein A agarose beads, washed five times with the extraction buffer, and eluted by boiling the beads in SDS-PAGE sample buffer. The eluted sample was resolved by 8% SDS-PAGE for western blotting.

Anti-KTF1 antibodies were generated by injecting rabbits with purified recombinant KTF1 protein (KTF1-P3) and were purified by affinity chromatography using KTF1-conjugated beads.

Immunofluorescence Microscopy

Interphase nuclei were isolated as described by Jasencakova et al. (2000). Nuclei preparations were postfixed with 4% paraformaldehyde and incubated overnight at 4°C with primary antibodies for KTF1 (1:50), anti-Flag (1:200, Sigma), or anti-cMyc (1:200, Chemicon). Secondary antibodies anti-rabbit Alexa 488 (Invitrogen) and anti-mouse Alexa 594 (Invitrogen) were diluted at 1:200 in PBS and incubated for 4 hr at 37°C. DNA was counterstained with 1 μg/ml DAPI in Prolong Gold mounting medium (Invitrogen). The nuclei preparations were analyzed with a Nikon Eclipse E80i epifluorescence microscope equipped with a Photometrics Coolsnap ES Mono digital camera. Images were acquired by the Phylum software and pseudocolored and merged in Adobe Photoshop.

Electrophoretic Mobility Shift Assay

NRPE1-CTD and various truncated forms of KTF1 cDNA were cloned into the pGEX4T1 vector (Invitrogen) for GST fusion constructs. The constructs were transformed into *E. coli* strain BL21 (Invitrogen) for protein expression. The GST fusion protein was purified by glutathione Sepharose 4B beads (Amersham) and used for electrophoretic mobility shift assay (EMSA). For the binding assay, single-stranded RNA or DNA probes were directly synthesized and end labeled with T4 polynucleotide kinase and γ-^{32}P-ATP, and the 500 nt single-stranded RNA probe was generated from the *RD29A* promoter sequence using an in vitro transcription-labeling kit (Ambion). All of the probes used for binding assays were purified using 50 G columns (Biolab). The binding reaction included 2 μl of labeled RNA or DNA probes, 0.5 μg of GST fusion protein, 25 mM HEPES (pH 7.6), 50 mM KCl, 0.1 mM EDTA (pH 8.0), 12.5 mM $MgCl_2$, 1 mM DTT, 0.5% (w/v) BSA, and 5% (w/v) glycerol. Reactions were incubated at room temperature for 30 min. The reaction mixtures were resolved on 4% nondenaturing polyacrylamide gel following electrophoresis at 200 V for 2 hr. Gels were dried and exposed to X-Ray film for analysis.

RNA-IP

The *ros1* and *ros1rdm3-1* were subjected to RNA immunoprecipitation with anti-KTF1 antibodies, following the method of Wierzbicki et al. (2008).

SUPPLEMENTAL DATA

Supplemental Data include seven figures and two tables and can be found with this article online at http://www.cell.com/supplemental/S0092-8674(09)00453-X.

ACKNOWLEDGMENTS

We thank Xuemei Chen and Shou-Wei Ding for helpful discussion. This work was supported by National Institutes of Health grants R01GM070795 and R01GM059138 to J.-K.Z., GM077590 to C.S.P., and National Science Foundation grant MCB-0642843 to H.J. O.P. was supported by an Edward Mallinckrodt Foundation Award.

Received: January 22, 2009
Revised: March 11, 2009
Accepted: April 13, 2009
Published: April 30, 2009

REFERENCES

Agius, F., Kapoor, A., and Zhu, J.K. (2006). Role of the Arabidopsis DNA glycosylase/lyase ROS1 in active DNA demethylation. Proc. Natl. Acad. Sci. USA *103*, 11796–11801.

Bartel, D.P. (2004). MicroRNAs: Genomics, biogenesis, mechanism, and function. Cell *116*, 281–297.

Buhler, M., Verdel, A., and Moazed, D. (2006). Tethering RITS to a nascent transcript initiates RNAi- and heterochromatin-dependent gene silencing. Cell *125*, 873–886.

Cao, X., and Jacobsen, S.E. (2002). Role of the arabidopsis DRM methyltransferases in *de novo* DNA methylation and gene silencing. Curr. Biol. *12*, 1138–1144.

Chan, S.W., Henderson, I.R., and Jacobsen, S.E. (2005). Gardening the genome: DNA methylation in Arabidopsis thaliana. Nat. Rev. Genet. *6*, 351–360.

Chen, E.S., Zhang, K., Nicolas, E., Cam, H.P., Zofall, M., and Grewal, S.I. (2008). Cell cycle control of centromeric repeat transcription and heterochromatin assembly. Nature *451*, 734–737.

Ding, L., and Han, M. (2007). GW182 family proteins are crucial for microRNA-mediated gene silencing. Trends Cell Biol. *17*, 411–416.

El-Shami, M., Pontier, D., Lahmy, S., Braun, L., Picart, C., Vega, D., Hakimi, M.A., Jacobsen, S.E., Cooke, R., and Lagrange, T. (2007). Reiterated WG/GW motifs form functionally and evolutionarily conserved ARGONAUTE-binding platforms in RNAi-related components. Genes Dev. *21*, 2539–2544.

Eulalio, A., Huntzinger, E., and Izaurralde, E. (2008). GW182 interaction with Argonaute is essential for miRNA-mediated translational repression and mRNA decay. Nat. Struct. Mol. Biol. *15*, 346–353.

Filipowicz, W. (2005). RNAi: The nuts and bolts of the RISC machine. Cell *122*, 17–20.

Gong, Z., Morales-Ruiz, T., Ariza, R.R., Roldan-Arjona, T., David, L., and Zhu, J.K. (2002). ROS1, a repressor of transcriptional gene silencing in Arabidopsis, encodes a DNA glycosylase/lyase. Cell *111*, 803–814.

He, X.J., Hsu, Y.F., Pontes, O., Zhu, J., Lu, J., Bressan, R.A., Pikaard, C., Wang, C.S., and Zhu, J.K. (2009). NRPD4, a protein similar to the RPB4 subunit of RNA polymerase II, is a component of RNA polymerases IV and V and is required for siRNA production, RNA-directed DNA methylation, and transcriptional gene silencing. Genes Dev. *23*, 318–330.

Huang, L., Jones, A.M., Searle, I., Patel, K., Vogler, H., Hubner, N.C., and Baulcombe, D.C. (2009). An atypical RNA polymerase involved in RNA silencing shares small subunits with RNA polymerase II. Nat. Struct. Mol. Biol. *16*, 91–93.

Irvine, D.V., Zaratiegui, M., Tolia, N.H., Goto, D.B., Chitwood, D.H., Vaughn, M.W., Joshua-Tor, L., and Martienssen, R.A. (2006). Argonaute slicing is required for heterochromatic silencing and spreading. Science *313*, 1134–1137.

Ivanov, D., Kwak, Y.T., Guo, J., and Gaynor, R.B. (2000). Domains in the SPT5 protein that modulate its transcriptional regulatory properties. Mol. Cell. Biol. *20*, 2970–2983.

Jasencakova, Z., Meister, A., Walter, J., Turner, B.M., and Schubert, I. (2000). Histone H4 acetylation of euchromatin and heterochromatin is cell cycle dependent and correlated with replication rather than with transcription. Plant Cell *12*, 2087–2100.

Kapoor, A., Agarwal, M., Andreucci, A., Zheng, X., Gong, Z., Hasegawa, P.M., Bressan, R.A., and Zhu, J.K. (2005). Mutations in a conserved replication protein suppress transcriptional gene silencing in a DNA-methylation-independent manner in Arabidopsis. Curr. Biol. *15*, 1912–1918.

Li, C.F., Pontes, O., El-Shami, M., Henderson, I.R., Bernatavichute, Y.V., Chan, S.W., Lagrange, T., Pikaard, C.S., and Jacobsen, S.E. (2006). An ARGONAUTE4-containing nuclear processing center colocalized with Cajal bodies in Arabidopsis thaliana. Cell *126*, 93–106.

Lindstrom, D.L., Squazzo, S.L., Muster, N., Burckin, T.A., Wachter, K.C., Emigh, C.A., McCleery, J.A., Yates, J.R., and Hartzog, G.A. (2003). Dual roles for Spt5 in pre-mRNA processing and transcription elongation revealed by identification of Spt5-associated proteins. Mol. Cell. Biol. *23*, 1368–1378.

Lippman, Z., May, B., Yordan, C., Singer, T., and Martienssen, R. (2003). Distinct mechanisms determine transposon inheritance and methylation via small interfering RNA and histone modification. PLoS Biol. *1*, E67.

Lister, R., O'Malley, R.C., Tonti-Filippini, J., Gregory, B.D., Berry, C.C., Millar, A.H., and Ecker, J.R. (2008). Highly integrated single-base resolution maps of the epigenome in Arabidopsis. Cell *133*, 523–536.

Matzke, M.A., and Birchler, J.A. (2005). RNAi-mediated pathways in the nucleus. Nat. Rev. Genet. *6*, 24–35.

Matzke, M., Kanno, T., Daxinger, L., Huettel, B., and Matzke, A.J. (2009). RNA-mediated chromatin-based silencing in plants. Curr. Opin. Cell Biol., in press. Published online February 23, 2009. 10.1016/j.ceb.2009.01.025.

Mosher, R.A., Schwach, F., Studholme, D., and Baulcombe, D.C. (2008). Pol IVb influences RNA-directed DNA methylation independently of its role in siRNA biogenesis. Proc. Natl. Acad. Sci. USA *105*, 3145–3150.

Partridge, J.F., DeBeauchamp, J.L., Kosinski, A.M., Ulrich, D.L., Hadler, M.J., and Noffsinger, V.J. (2007). Functional separation of the requirements for establishment and maintenance of centromeric heterochromatin. Mol. Cell *26*, 593–602.

Penterman, J., Zilberman, D., Huh, J.H., Ballinger, T., Henikoff, S., and Fischer, R.L. (2007). DNA demethylation in the Arabidopsis genome. Proc. Natl. Acad. Sci. USA *104*, 6752–6757.

Pontes, O., Li, C.F., Nunes, P.C., Haag, J., Ream, T., Vitins, A., Jacobsen, S.E., and Pikaard, C.S. (2006). The Arabidopsis chromatin-modifying nuclear siRNA pathway involves a nucleolar RNA processing center. Cell *126*, 79–92.

Qi, Y., He, X., Wang, X.J., Kohany, O., Jurka, J., and Hannon, G.J. (2006). Distinct catalytic and non-catalytic roles of ARGONAUTE4 in RNA-directed DNA methylation. Nature *443*, 1008–1012.

Ream, T.S., Haag, J.R., Wierzbicki, A.T., Nicora, C.D., Norbeck, A., Zhu, J.K., Hagen, G., Guilfoyle, T.J., Pasa-Tolic, L., and Pikaard, C.S. (2009). Subunit compositions of the RNA-silencing enzymes Pol IV and Pol V reveal their origins as specialized forms of RNA polymerase II. Mol. Cell *33*, 192–203.

Till, S., Lejeune, E., Thermann, R., Bortfeld, M., Hothorn, M., Enderle, D., Heinrich, C., Hentze, M.W., and Ladurner, A.G. (2007). A conserved motif in Argonaute-interacting proteins mediates functional interactions through the Argonaute PIWI domain. Nat. Struct. Mol. Biol. *14*, 897–903.

Tomari, Y., and Zamore, P.D. (2005). Perspective: Machines for RNAi. Genes Dev. *19*, 517–529.

Verdel, A., Jia, S., Gerber, S., Sugiyama, T., Gygi, S., Grewal, S.I., and Moazed, D. (2004). RNAi-mediated targeting of heterochromatin by the RITS complex. Science *303*, 672–676.

Volpe, T.A., Kidner, C., Hall, I.M., Teng, G., Grewal, S.I., and Martienssen, R.A. (2002). Regulation of heterochromatic silencing and histone H3 lysine-9 methylation by RNAi. Science *297*, 1833–1837.

Wada, T., Takagi, T., Yamaguchi, Y., Ferdous, A., Imai, T., Hirose, S., Sugimoto, S., Yano, K., Hartzog, G.A., Winston, F., et al. (1998). DSIF, a novel transcription elongation factor that regulates RNA polymerase II processivity, is composed of human Spt4 and Spt5 homologs. Genes Dev. *12*, 343–356.

Wierzbicki, A.T., Haag, J.R., and Pikaard, C.S. (2008). Noncoding transcription by RNA polymerase Pol IVb/Pol V mediates transcriptional silencing of overlapping and adjacent genes. Cell *135*, 635–648.

Wierzbicki, A.T., Ream, T.S., Haag, J.R., and Pikaard, C.S. (2009). RNA polymerase V transcription guides ARGONAUTE4 to chromatin. Nat. Genet., in press. Published online April 19, 2009. 10.1038/ng.365.

Winston, F. (2001). Control of eukaryotic transcription elongation. Genome Biol. *2*, REVIEWS1006.

Yamada, T., Yamaguchi, Y., Inukai, N., Okamoto, S., Mura, T., and Handa, H. (2006). P-TEFb-mediated phosphorylation of hSpt5 C-terminal repeats is critical for processive transcription elongation. Mol. Cell *21*, 227–237.

Zaratiegui, M., Irvine, D.V., and Martienssen, R.A. (2007). Noncoding RNAs and gene silencing. Cell *128*, 763–776.

Zhang, X., Henderson, I.R., Lu, C., Green, P.J., and Jacobsen, S.E. (2007). Role of RNA polymerase IV in plant small RNA metabolism. Proc. Natl. Acad. Sci. USA *104*, 4536–4541.

Zhang, K., Mosch, K., Fischle, W., and Grewal, S.I. (2008). Roles of the Clr4 methyltransferase complex in nucleation, spreading and maintenance of heterochromatin. Nat. Struct. Mol. Biol. *15*, 381–388.

Zheng, X., Zhu, J., Kapoor, A., and Zhu, J.K. (2007). Role of Arabidopsis AGO6 in siRNA accumulation, DNA methylation and transcriptional gene silencing. EMBO J. *26*, 1691–1701.

Zhu, J., Kapoor, A., Sridhar, V.V., Agius, F., and Zhu, J.K. (2007). The DNA glycosylase/lyase ROS1 functions in pruning DNA methylation patterns in Arabidopsis. Curr. Biol. *17*, 54–59.